Enhancing the Catalysis of Oxygen Reduction Reaction via Tuning Interfacial Hydrogen Bonds

Tao Wang
Massachusetts Institute of Technology
Yirui Zhang
Massachusetts Institute of Technology https://orcid.org/0000-0001-7604-8623
Botao Huang
MIT
Bin Cai
Pacific Northwest National Laboratory
Reshma Rao
Imperial College London https://orcid.org/0000-0002-6655-3105
Livia Giordano
MIT
Shi-Gang Sun
Xiamen University
Yang Shao-Horn (shaohorn@mit.edu)
MIT https://orcid.org/0000-0001-8714-2121

Article

Keywords: proton-coupled electron transfer, oxygen reduction reaction, hydrogen bonds

Posted Date: December 15th, 2020

DOI: https://doi.org/10.21203/rs.3.rs-115124/v1

Version of Record: A version of this preprint was published at Nature Catalysis on September 6th, 2021.
See the published version at https://doi.org/10.1038/s41929-021-00668-0.

Enhancing the Catalysis of Oxygen Reduction Reaction via Tuning Interfacial Hydrogen Bonds

Tao Wang[1,4,5†], Yirui Zhang[1,2†], Botao Huang[1,4], Bin Cai[1,2], Reshma Rao[1,4], Livia Giordano[1,2], Shi-Gang Sun[5], Yang Shao-Horn[1,2,3,4*]

[1]Electrochemical Energy Laboratory, Massachusetts Institute of Technology Cambridge, MA 02139, USA

[2]Department of Mechanical Engineering, Massachusetts Institute of Technology Cambridge, MA 02139, USA

[3]Department of Materials Science and Engineering, Massachusetts Institute of Technology Cambridge, MA 02139, USA

[4]Research Laboratory of Electronics, Massachusetts Institute of Technology 77 Massachusetts Avenue, Cambridge, MA 02139, US

[5]Collaborative Innovation Center of Chemistry for Energy Materials, State Key Laboratory for Physical Chemistry of Solid Surfaces, College of Chemistry and Chemical Engineering, Xiamen University, Xiamen, 361005, China

[†]These authors contributed equally: Tao Wang, Yirui Zhang

*Correspondence: shaohorn@mit.edu

Abstract:

Proton activity at the electrified interface is central to the kinetics of proton-coupled electron transfer (PCET) reactions for making chemicals and fuels. Here we employed a library of protic ionic liquids in an interfacial layer on Pt and Au to alter local proton activity, where the intrinsic ORR activity was enhanced up to 5 times, exhibiting a

volcano-shaped dependence on the pK_a of the ionic liquid. The enhanced ORR activity was attributed to favorable proton transfer kinetics for strengthened hydrogen bonds between the ionic liquid to the ORR product with comparable pK_a. This proposed mechanism was supported by *in situ* surface-enhanced Fourier-Transform Infrared Spectroscopy and our simulation of PCET kinetics based on computed proton vibrational wavefunction at the H-bond interface. These findings highlight opportunities in using non-covalent interactions of hydrogen bond structures and solvation environments at the electrified interface to tune the kinetics of ORR and beyond.

Understanding proton coupled electron transfer (PCET) processes are critical to control the reaction kinetics in bio-[1, 2, 3], organic[2, 4], inorganic[5, 6, 7], environmental chemistry [8] and electrochemistry[4, 9]. In particular, PCET steps have been used extensively in recent research on catalysts for making energy carriers or solar fuels[4, 10, 11, 12] including water splitting[4, 12, 13], and for converting energy carriers in fuel cells to generate work[7, 9] including oxygen reduction reaction (ORR)[9]. Current thinking of the ORR mechanism[9, 14] involves PCET steps on surface metal sites, which can involve one key intermediate on metals such as Au[15] for two-electron ORR ($O_2 + 2H^+ + 2e^- \rightarrow H_2O_2$, 0.68 V_{RHE}), -OOH[15, 16, 17], and three key intermediates on metals such as Pt[14, 18, 19], -OOH, -O and -OH for four-electron ORR ($O_2 + 4H^+ + 4e^- \rightarrow 2H_2O$, 1.23 V_{RHE})[20]. Conventional designs of catalysts involve the tuning of the surface electronic structure and covalent interactions with reaction intermediates[14, 20, 21] (surface binding or adsorption strength), which has led to significant advances in the intrinsic ORR activity by tuning strain[22, 23], the ligand effect[24, 25], and surface orientation.[26, 27, 28] For example, $Pt_3Ni(111)$[29] is shown to exhibit intrinsic ORR activity ten times greater than Pt (111) at 0.9 V_{RHE}, and

polycrystalline PtGd[30] exhibit five times enhancement than polycrystalline Pt.

Recent studies[31, 32, 33, 34, 35, 36, 37, 38, 39, 40, 41] have shown that changing electrolyte compositions can significantly alter the kinetics of electrochemical reactions such as oxygen reduction reaction (ORR) [31, 32, 34, 35, 38, 39] and hydrogen oxidation reaction[33, 36, 37, 40, 41], highlighting new opportunities in noncovalent interactions via the chemical physics of electrolytes to control activity. While the pH of electrolyte, which represents proton activity, does not greatly alter the ORR activity of metals such as Pt[42], increasing pH can significantly increase the ORR activity on weakly interacting metals such as Au[43, 44, 45, 46], where the activity in base is much higher than that in acid[44]. Moreover, modifying Pt-based catalysts with protic ionic liquids[32, 47, 48] is shown to enhance the ORR activity in acid, where ionic-liquid-modified PtNi nanoparticles have ~3 times greater intrinsic ORR activity than pristine PtNi[32], and ~20 times greater than commercial Pt/C[48]. Although this increase in the ORR activity has been attributed to the increase of hydrophobicity at the interface between Pt and ionic liquids[47, 49] and oxygen solubility in ionic liquids[32, 50], it is not apparent on how to design new catalysts to control the catalytic activity of ORR and other reactions using this strategy. Considering these ionic liquids used in these previous studies[32, 47, 48] have different pK_a from the acidic electrolyte, it is postulated that interfacial proton activity of ionic liquids can alter proton transfer or proton-coupled electron transfer (PCET) kinetics on metals such as Pt and Au, and thus ORR activity, which is the focus of this work.

Here we employ a library of protic ionic liquids in an interfacial layer to tune ORR kinetics of Pt and Au in acid. We hypothesize that the protic cations in the ionic liquids

can serve as intermolecular proton relay between proton in the bulk electrolyte and that near the metal surface (Scheme 1), where altering of protic cation with different proton activity (or pK_a) provides opportunities to examine how local proton activity near the active sites can influence the ORR kinetics. A library of protic cations with different pK_a values were used (Scheme 1) $[C_4C_1im]^+$ pK_a=23.3[51], $[TMPim]^+$ pK_a=21.3[51], $[MTBD]^+$ pK_a=15.0[52], $[DBU]^+$ pK_a=13.5[52], $[DEMA]^+$ pK_a=10.3[53], $[TEMEDA]^+$ pK_a=8.9[54], $[C_4Him]^+$ pK_a=7.1[55] to influence the ORR activity of Au and Pt, which catalyzes ORR via the $2e^-$ [45] and $4e^-$ [56] pathway in acid, respectively. The ORR activity of Au and Pt was found to increase with the presence of protic cations, where the maximum enhancement was obtained when the pK_a values of protic cations and the reaction intermediate in the ORR rate-limiting step are similar. The ORR activity enhancement can be attributed to the stronger hydrogen bond between protic cations and the rate-limiting ORR intermediate, which is supported by *in situ* attenuated total reflection surface-enhanced infrared absorption spectroscopy (ATR-SEIRAS). Further support came from predicted PCET kinetics based on computed proton vibrational wavefunction at the H-bond interface, where the stronger H-bond between protic cations and ORR intermediates led to faster proton tunneling kinetics, giving rise to greater ORR exchange current density. Our work reveals the role of local pK_a and interfacial H-bond strength on the kinetics of PCET and electrochemical reactions, which highlight new opportunities to further enhance electrocatalytic activity of ORR, reduction of CO_2 and N_2, and beyond by tuning how local proton activity near the active sites.

pK_a-dependent ORR activity measurements of protic-cation-modified catalysts

The ORR activity of Au/C (6.0 nm Au) and Pt/C (TKK, 19wt% 1.7 nm Pt) with and without protic cations was measured using rotating disk electrode measurements, as shown in Fig. 1a and 1b, respectively. The ionic liquid layer thickness with protic cations on the surface of Au/C and Pt/C was estimated to ~1 nm (details in Fig. S1). The catalysts with protic cations showed enhanced activity compared to those without, as indicated by the positive shifts in the half-wave potential in the voltammetry data. ORR kinetic currents were extracted from the data in Fig. 1a, 1b and Fig. S2 using the Koutecky–Levich analysis, from which the specific and mass activity was obtained by normalizing the kinetic ORR current (Fig. S3) by the electrochemically surface area from CV measurements (Fig. S4-5) and metal mass (Fig. S6), respectively. The specific ORR activity for Au/C at 0.4 V_{RHE} can be enhanced up to ~5 times with protic cations relative to pristine Au/C shown in this work while that of Pt/C at 0.9 V_{RHE} can be increased by ~3 times compared to pristine Pt/C (TKK 19%, ~190 $\mu A/cm^2_{Pt}$) shown in this work and previous studies[57, 58, 59, 60, 61]. Similar activity trends and enhancement were found for polycrystalline Au (~4 times at 0.3V_{RHE}, Fig. S7a) and Pt (~2 times at 0.9 V_{RHE}, Fig. S7b). The exchange current density of ORR was extracted for Au/C ($O_2 + 2H^+ + 2e^- \Rightarrow H_2O_2$, 0.68 V_{RHE}) and for Pt/C ($O_2 + 4H^+ + 4e^- \Rightarrow 2H_2O$, 1.23 V_{RHE}) using Butler-Volmer in Fig. S8 and Fig. S9 respectively. These observations suggest that the local proton activity at the metal/electrolyte interface can considerably influence the ORR kinetics.

The ORR activity of both Au/C and Pt/C was found to first increase and then decrease, exhibiting a volcano trend, as a function of the pK_a value of protic cations, as shown in Fig. 1c and Fig. 1d, respectively. The maximum ORR activity enhancement for Au/C was found for [DEMA][NTf_2] with pK_a of 10.3, which is similar to the ORR product on Au , H_2O_2 of pK_a of 11.6 [62]. In acid, the first PCET step of ORR on Au ($O_2 + H_3O^+$

+ e^- => OOH_{Au} + H_2O) has similar kinetics to the second step (OOH_{Au} + H_3O^+ + e^- => H_2O_2 + H_2O), as indicated by the 0.09 eV difference in activation barrier from DFT[21, 63]. As increasing pH is shown to promote the rate of the first step by several orders of magnitude[46], the second step becomes rate-limiting to the overall kinetics with increasing pH. Therefore, we propose that the ORR kinetics on Au with interfacial ionic liquids are limited by the PCET kinetics of OOH_{Au} to form H_2O_2 (OOH_{Au} + N-H^+ + e^- => H_2O_2 + N)[15, 21] (the detailed kinetic analysis depicted in Fig. S10). This hypothesis is in agreement with previous kinetic measurements of ORR in organic solvents, where the first electron transfer step (O_2 + e^- => O_2^-) [64] is more than 10^3 times faster than the second PCET step (O_2^-+ e^- + H_2O => OOH^- + OH^-)[65]. Further support comes from the observation that OOH_{Au} has been detected as the stable ORR intermediate accumulating on Au by *in situ* ATR-SEIRAS[16, 17] and *in situ* surface enhanced Raman[66]. Therefore, it is proposed that different pK_a altered the kinetics of the second PCET step for ORR on Au in ionic liquid (OOH_{Au} + N-H^+ + e^- => H_2O_2 + N) and tuned the overall ORR kinetics consequently. This hypothesis departs from the decoupled proton-electron transfer mechanism outlined by Koper,[9, 41] where increasing kinetics with increasing pH for one-electron reduction can be attributed to enhanced electron-transfer kinetics on the RHE scale.

The maximum ORR activity enhancement for Pt/C occurred for [MTBD][NTf_2] with pK_a of 15.0, which is similar to the ORR product in the rate-limiting step, water with pK_a of 15.7 [62]. Previous DFT studies have shown that PCET of adsorbed OH on Pt to form H_2O is rate-limiting (OH_{Pt} + H^+ + e^- => Pt + H_2O),[14] which is supported by ambient pressure X-ray photoelectron spectroscopy[18] and *in situ* electrochemical surface-enhanced Raman spectroscopy[19]. Therefore, these results show that the kinetics of ORR on Au and Pt could be regulated by the pK_a of protic cations at the interface,

which can work as the proton donor near the active sites catalyzing the rate-limiting PCET, having the maximum ORR activity obtained with minimum pK_a difference between the protic ionic liquid (proton donor) and rate-limiting ORR product (proton acceptor).

As the thermodynamic driving force of proton coupled electron transfer (PCET) reactions diminishes with minimized pK_a difference between the proton donor and acceptor[67], we propose that the enhancement in the ORR activity can be attributed to difference in the interfacial hydrogen bond structure as predicted previously by PCET theory for homogeneous reactions[5, 6, 7], which will be examined by *in situ* ATR-SEIRAS experiments and computation below.

pK_a-dependent interfacial H-bond detected by *in situ* ATR-SEIRAS

In situ ATR-SEIRAS was performed on Au and Pt thin-film chemically deposited on Si prism, which detected ORR intermediates and revealed the interactions between protic cations in ionic liquids and ORR intermediates by monitoring the stretching frequency of H-bonded species of protic cations as influenced by the formation of ORR intermediates and product as a function of potential. Potential-dependent *in situ* ATR-SEIRA spectra were collected from [MTBD][NTf_2]-modified Au thin-film surface (estimated to have a thickness of ~ 50 nm for Au and ~20 μm for [MTBD][NTf_2]). Differential spectra subtracted by that collected at OCV are shown in Fig. 2, along with that of bulk [MTBD][NTf_2] and [MTBD][NTf_2] with water (0.5 M water). Two sharp peaks at 1632 cm^{-1} and 1603 cm^{-1} (Fig. 2a), resulting from the stretching mode of C=N-H^+ and C=N in the cation[68], respectively, grew with decreasing potential. The increased peak intensities can be attributed to having more protic cations on the Au surface with decreasing potential, which is in agreement with increasing peak intensities of C-N

stretching[69, 70] from protic cations at 1231 cm^{-1} (Fig. 2b). Similar peaks to those found on Au were found on [MTBD][NTf_2]-modified Pt thin-film surface (Fig. S11), which also grew with decreasing potential.

Two new peaks, at 1263 cm^{-1} and 3238 cm^{-1} emerged (Fig. 2b and 2c) with decreasing potential, which can be assigned to the bending (H-O-O) of HOO-adsorbed on Au[16, 17] and the stretching of N-H^+···OOH_{Au} of [MTBD][NTf_2], respectively. The assignment of the broad feature at 3238 cm^{-1} is supported by DFT calculations, where computed N-H^+···OOH_{Au} stretching of [MTBD][NTf_2] was determined to be 3267 cm^{-1} (Table S1), in good agreement with the experimental observation. This new broad peak at ~3238 cm^{-1} is redshifted compared to the N-H^+ stretching of bulk [MTBD][NTf_2] with and without water added (~3400 cm^{-1} in Fig. 2c), indicating the presence of hydrogen bond interactions between protic cation and ORR intermediates such as [MTBD]N-H^+···OOH_{Au}. These two peaks at 1263 cm^{-1} and 3238 cm^{-1} grew at the expense of the peak at 3583 cm^{-1}, attributable to the O-H stretching[71] of water dissolved in the [MTBD][NTf_2] in Fig. 2c and Fig. S11, which indicated reduction of water adsorbed on the surface with decreasing potential.

Changing the pK_a of protic cations was found to redshift the N-H^+···OOH_{Au} stretching at ORR-relevant potentials (Fig. 3 and Fig. S12 and 13). The N-H^+···OOH_{Au} stretching frequency decreased from 3429 cm^{-1} for [C_4Him][NTf_2] with pK_a of 7.1 in Fig. 3c, 3238 cm^{-1} for [MTBD][NTf_2] with pK_a of 15.0 in Fig. 3a, to ~3000 cm^{-1} for [DEMA][NTf_2] with pK_a of 10.3 in Fig. 3b, at 0.2 V_{RHE}. These assignments are supported by DFT calculations (Table S1), which also show the two fine peak features at ~3000 cm^{-1} for [DEMA][NTf_2] with the maximum ORR activity, having the feature at 2985 cm^{-1} to the stretching of [DEMA]N-H^+···OOH_{Au} and the feature at 3024 cm^{-1} to [DEMA]N-H^+···OHOH. Further support to these assignments came from the observed peak growth

as expected for increasing ORR intermediates with decreasing potential (Fig. S12, S13 and S14). Weakening the N-H^+ (proton donor) stretching of N-$H^{+}\cdots OOH_{Au}$ from [C_4Him][NTf_2] to [DEMA][NTf_2] indicates stronger hydrogen bond interactions in N-$H^{+}\cdots OOH_{Au}$ as shown from previous IR spectroscopy studies of hydrogen-bonded (H-Bond) species[72, 73], suggesting the strongest hydrogen bond found for [DEMA][NTf_2] with a similar pK_a (10.3) to H_2O_2 (11.6). This observation is in agreement with general trends that the H-bond would become stronger when the difference between the pK_a value of proton donor and acceptor decreases as shown from thousands of H-bond structures from the Cambridge Structural Database including the N-$H^{+}\cdots$O, N-$H^{+}\cdots$N etc.[74] Therefore, the maximum ORR activity found on Au in presence of [DEMA][NTf_2] is associated with the strongest H-bond interaction between N-$H^{+}\cdots$OOH (Fig. 3g). Considering the rate of ORR on Au is limited by PCET from OOH_{Au} to form H_2O_2 on Au in ionic liquids (OOH_{Au} + N-H^+ + e^- = H_2O_2 + N), strengthening H$\cdots$OOH facilitated by protic cations with comparable pK_a such as [DEMA]N-H^+ would enhance ORR kinetics.

Similar to Au, the maximum ORR activity found on Pt in presence of [MTBD][NTf_2] is associated with the strongest H-bonding interaction between N-H^+ and OH of species such as N-$H^{+}\cdots OH_{Pt}$ among the protic cations examined in this study, as shown in Fig. 3d-f, Fig. 3h and Fig. S15-17. This assignment is in agreement with the detection of Pt-OH as the dominant ORR intermediate by *in situ* SERS and XPS[18, 19] and previous DFT findings that PCET of OH adsorbed on Pt is rate-limiting for ORR[68, 75]. Further support came from the agreement between experimentally observed and DFT calculated (Table S1) wavenumber for N-H^+ stretching, where the computed value for [MTBD]N-$H^{+}\cdots OH_{Pt}$, [DEMA]N-$H^{+}\cdots OH_{Pt}$ and [C_4Him]N-$H^{+}\cdots OH_{Pt}$ was found to be 3089 cm^{-1}, 3188 cm^{-1} and 3335 cm^{-1}, respectively. Like Au, the N^+-H stretching for the protic

cation with the maximum ORR activity has one additional feature to [MTBD]N-$H^+\cdots OH_{Pt}$ at 3089 cm^{-1}, which can be attributed to [MTBD]N-$H^+\cdots OH_2$ at 3215 cm^{-1} as supported by DFT (Table S1), revealing the presence of the ORR intermediate (OH_{Pt} and final product (H_2O) in the rate-limiting step. Considering the PCET from OH_{Pt} to form H_2O (OH_{Pt} + N-H^+ + e^- = H_2O + N) is rate-limiting, strengthening H···OH facilitated by protic cations with comparable pK_a such as [MTBD]N^+-H would enhance ORR kinetics.

pK_a-dependent PCET kinetics in ORR facilitated by protic cations

Here we compute the exchange current densities of PCET kinetics (Fig. 4a) from select protic cations in the rate-limiting ORR step on Au (N-$H^+\cdots OOH_{Au}$ + e^- => H_2O_2 + N) and Pt (N-$H^+\cdots OH_{Pt}$ + e^- => H_2O + N) using reported methods.[5, 7, 76] While the minimum point of proton potential is close to proton donor side (e.g. N atom of N-$H^+\cdots OOH_{Au}$) before electron transfer, the reaction intermediate (such as adsorbed OOH or OH) accepts one electron from electrode and lowers the proton potential, enabling proton transfer to form product, where proton is assumed to transferred simultaneously with electron[5, 76]. The transferring proton was treated by quantum mechanics[76] and the proton vibronic states were computed from the proton potentials of [MTBD]N-$H^+\cdots OOH_{Au}$ (Fig. S18a), [DEMA]N-$H^+\cdots OOH_{Au}$ (Fig. S18b), [C_4Him]N-$H^+\cdots OOH_{Au}$ (Fig. S18c), [MTBD]N-$H^+\cdots OH_{Pt}$ (Fig. S18d), [DEMA]N-$H^+\cdots OH_{Pt}$ (Fig. S18e) and [C_4Him]N-$H^+\cdots OH_{Pt}$ (Fig. S18f), where the wavefunctions and energy levels of different quantum states are shown in Fig. S19-S24. The PCET reaction was described regarding the transition between vibrational states[76] of reactant (e.g. N-$H^+\cdots OOH_{Au}$) and product (e.g.

H_2O_2), where the exchange current density was proportional to the product of the vibronic coupling squared. Here we assume that the electronic coupling is unchanged for ORR with different protic cations as the distance between reaction intermediate (adsorbed OOH and OH) and electron donor (electrode surface, Au and Pt) remains constant[7]. Therefore, we will focus on the H-bonding structure effect on overall PCET kinetics in this part, the exchange current density is proportional to the product of the vibronic coupling of proton squared (denoted as $S_{v\mu}^2$)[5], the Boltzmann probability of different proton vibrational states (P_v)[5] and the Boltzmann probability overcoming the activation free energy ($\Delta G^{\ddagger}$) in Fig. 4b. As summarized in Table S10 and S11, where one or two states dominate the overall kinetics, showing much higher rate constant than others, the differences in $\Delta G^{\ddagger}$ of contributing states of [MTBD]N-$H^+\cdots OOH_{Au}$, [DEMA]N-$H^+\cdots OOH_{Au}$, [C_4Him]N-$H^+\cdots OOH_{Au}$ are within 0.05 eV. Similarly, the differences in $\Delta G^{\ddagger}$ (Table S11) of contributing states of [MTBD]N-$H^+\cdots OH_{Pt}$, [DEMA]N-$H^+\cdots OH_{Pt}$, [C_4Him]N-$H^+\cdots OH_{Pt}$ are within 0.04 eV. These results indicate the effect of $\Delta G^{\ddagger}$ on the PCET kinetics is insignificant in this work, while the enhancement in ORR exchange current density mainly resulted from the H-bonding structure, regulating the tunneling kinetics of PCET and tuning the pre-exponential factor in the rate constant expression.

Our computational results show that the enhancement in the ORR activity of Au and Pt by the presence of protic cations with select pK_a can be attributed to greater $P_v S_{v\mu}^{\ 2}$ of protons across the contributing states (Fig. 4e and 4f). $S_{v\mu}^2$ was quantified by the integral overlap of proton vibrational wavefunctions between reactant (oxidized state, before

ET) and product (reduced state, after ET) (Table S8) indicating the vibronic coupling of proton through PCET process and P_v as the Boltzmann probability of different quantum states is shown in Table S9. As shown in Fig. 4c, the energy of reactant higher states for N-H^+···OOH_{Au} than the ground state (state 0) is much higher (0.35-0.4 eV in Table S8), so the (0, 0) transition is the contributing state for overall kinetics, the PCET kinetics are dominated by the vibronic coupling of protons across the ground states of reactant to product (0,0), having P_v of ground state close to 1 in Table S8. $P_vS_{v\mu}^2$ and exchange current density (J_0) for [DEMA]N-H^+···OOH_{Au} was found higher than [C_4Him]N-H^+···OOH_{Au} and [MTBD]N-H^+···OOH_{Au} in Fig. 4d and Table S10, which is in agreement with experimental results (Fig. 1). In contrast to Au, as the energy of state 1 for reactant of N-H^+···OH_{Pt} is only 0.1-0.2 eV higher than the ground state (Table S9), and proton wavefunction of reactant in state 1 distributes more on oxygen side (Fig. 4e) which can generate much higher vibronic coupling in (1, 0) transition state than (0, 0) to compensate the decrease in P_v of state 1, leading (1, 0) transition become contributing state for PCET kinetics in N-H^+···OH_{Pt}. Since the $S_{v\mu}$ (0,1) being similar for different ionic liquids in Table S9, the PCET kinetics are governed by the P_v of protons across the state 1. $P_vS_{v\mu}^2$ and exchange current density (J_0) for [MTBD]N^+-H···OH_{Pt} was found the highest, in agreement with experimental exchange current density trends, as shown in Fig. 4f and Table S11. Therefore, increasing ORR activity of Au and Pt by the presence of protic cations can be attributed to greater $P_vS_{v\mu}^2$ of protons across the contributing states, peaked at [DEMA]N-H^+···OOH_{Au} with comparable pK_a between [DEMA]N-H^+ and H_2O_2, and [MTBD]N-H^+···OH_{Pt} with comparable pK_a between

[MTBD]N-H^+ and H_2O, respectively. The predicted J_0 is in good agreement with those measured experimentally (Table S10 and S11). As the P_v and $S_{v\mu}$ reflect the properties of H-bonds vibronic states between selected protic cations and ORR intermediates, we reason that the kinetics of PCET relevant step on Au and Pt can be tuned by altering H-bond structures at the interface. This concept reflects the "Polanyi rules" discovered in fundamental reaction dynamic studies, which describes that vibrational energies play the most important role in the late-barrier atom-diatom reactions (H + X_2 => HX + X, X=Cl, Br)[77, 78]. This mechanism stands apart from previous studies on homogeneous reaction rates such as nitrogen reduction[79], hydrogen evolution[80, 81] and CO_2 reduction[82], where pK_a-dependent kinetics has been attributed largely to the driving force of proton (chemical potential) and electron (electro-potential tuned by redox potential of metal center) and pK_a-dependent activation energy. Therefore, we propose that the stretching frequency and $P_vS_{v\mu}^2$ of a H-bond, describing the vibrational features of intermediates, can be considered as descriptors for PCET kinetics. This study highlights the important role of vibrational features on reaction kinetics and new opportunities into electrolyte and interface tuning to control reaction kinetics.

Conclusions

This study shows that ORR activity forms a volcano relationship with pK_a of ion liquids (serving as proton donor) on the surface of Au and Pt in acid. The optimized pK_a for proton donor is around 15 and close to the pK_a value of water for Pt while the optimized pK_a for proton donor on Au is around 11 and close to the pK_a value of H_2O_2. *In situ* ATR-SEIRAS provides direct evidence for red-shifted stretching frequency of

X-H with decreasing ΔpK_a, which is associated with enhanced ORR activity. The effect of the H-bond structure on the kinetics of PCET is examined by the Boltzmann probability (P_v) and vibronic coupling of proton ($S_{v\mu}$) in different quantum states. Our results reveal that stronger H-bond can increase proton tunneling kinetics ($P_v S_{v\mu}^2$) by ~10-10^3 times whereas the activation free energy ($\Delta G^{\ddagger}$) of reaction remains largely unchanged. This work shows compelling evidence for pK_a-dependent hydrogen bond structures and their impact on the kinetics of proton tunneling and the rate-limiting PCET of ORR on Pt and Au, where altering the pK_a of proton donor at the catalyst surface can change the H-bonding interaction with ORR intermediates. Our findings highlight new opportunities beyond conventional catalyst design strategies of surface electronic structure tuning to control catalytic activity by tuning H-bond structures and/or solvation environments at the electrified interface.

Material and Methods

Pt/C and Au/C and Ag/C catalysts:

Pt/C catalysts was supplied by Tanaka Kikinzoku (TKK TEC10E20A), with weight fraction 19%. The Au nanoparticles were synthesized following a reported approach. [83] Briefly, Tetralin (10 mL), Oleylamine (OAm) (10 mL), and $HAuCl_4 \cdot 3H_2O$ (0.1 g) were mixed at room temperature and magnetically stirred for 10 min under N_2 atmosphere to make precursor solution. Then, the reducing solution of 0.5 mmol of TBAB, tetralin (1 mL), and OAm (1 mL) was injected into the precursor solution, the reaction was carried out with water-ice bath to maintain the temperature at 2 ºC for 1 h. After reaction, the nanoparticles were wash with acetone and collected by centrifugation. As prepared Au nanoparticles and carbon black were dispersed in solvent 1:1 isopropanol and hexane by 20-minute ultrasonicate treatment to synthesize the Au/C catalysts, resulting in 30wt.%

Au loading. The products were collected by centrifugation. To remove the residual surfactant, the loaded nanoparticles were heated at 200 °C for 0.5 h under the Ar atmosphere.

Synthesis of ionic liquids

The $[C_4C_1im][NTf_2]$(1-butyl-3-methylimidazolium bis(trifluoromethanesulfonyl)imide CAS No: 174899-83-3) was purchased from Sigma Aldrich. [TMPim][NTf2] 1,3-Bis(2,4,6-trimethylphenyl)imidazolium bis(trifluoromethanesulfonyl)imide was synthesized by the reported anion exchange reaction.[84] $Li[NTf_2]$ aqueous solution was added to [TMPim]Br slowly, which also dissolved in water. After the reaction, the IL would form a separated phase beneath the water phase. The product was washed by ultrapure water, and add 0.1M $AgNO_3$ to test the trace residual Br^- in the aqueous layer. The ionic liquid was washed until the $AgNO_3$ test was negative. The resulting product was dried by high vacuum at 80°C for 24 h., $[MTBD][NTf_2]$(1,3,4,6,7,8-Hexahydro-1-methyl-2H-pyrimido[1,2-a]pyrimidinebis(trifluoromethanesulfonyl)imide), $[DBU][NTf_2]$(2,3,4,6,7,8,9,10-Octahydropyrimidol[1,2-a]azepine bis(trifluoromethanesulfonyl)imide), [DEMA][NTf2](N,N-diethylmethylamine bis(trifluoromethanesulfonyl)imide, $[TEMEDA][NTf_2]$ (N,N,N′,N′-tetramethylethylenediamine bis(trifluoromethanesulfonyl)imide), $[C_4Him][NTf_2]$ (1-butyl-imidazolium bis(trifluoromethanesulfonyl)imide) were prepared through neutralization reactions in accordance with a previous report.[85] The MTBD, DBU, DEMA, TEMEDA and C_4Him aqueous solution was added to $HNTf_2$ solution slowly with cooling by ice bath. The products would form a separated phase beneath the water phase which was washed by ultrapure water several times and dried by high vacuum at 80 °C for 24 h.

Synthesis of ionic-liquid-modified catalysts

The ionic-liquid-modified catalysts were synthesized by a reported protocol[47]. Briefly, 90 mg M/C (M=Pt, Au, 19wt.% TKK Pt/C, as prepared 30wt.% Au/C were adopted) was mixed with 10mL iso-propyl alcohol solution containing a calibrated amount of IL (corresponding to a final IL loading of 16 wt%) with stirring at room temperature. After a 20-minute ultrasonic treatment, the solvent was evaporated under a low vacuum condition firstly and then dried under high vacuum at 80 °C for 24 h.

Electrochemical characterization

All the electrochemical measurements were performed using Biologic SP-300 potentiostat with a three-electrode electrochemical system. The working electrode was a glassy carbon rotating disk electrode (0.196 cm^2). The slurry was deposited on the working electrode, which consisted of 5 mg M/C (M=Pt, Au) and 5 mL mixture of deionized water, isopropyl alcohol, and 5 wt % Nafion solution in a volume ratio of 4:1:0.025. The loading of Pt was controlled at 20 $\mu g \cdot cm^{-2}$ and the loading of Au and Ag were controlled at 40 $\mu g \cdot cm^{-2}$. The electrolyte was prepared from Milli-Q water (18 MΩ•cm) and $HClO_4$ (70%, 99.999% trace metals basis). The SCE potential scale was calibrated with the RHE scale using H_2 electro-oxidation. All measurements were collected under Ar or O_2 saturation (ultra-high-grade purity, Airgas). The specific kinetic activity (J_k ($mA/cm^2_{Au\ or\ Pt}$)) of Au/C and Pt/C samples was calculated from Koutecky-Levich equation and electrochemical surface area determined by cyclic voltammetry, the detailed methods were depicted in SI.

In situ Surface Enhanced Infrared Absorption Spectroscopy (SEIRAS) Experiments.

For the *in situ* SEIRAS measurements, we used a working electrode composed of a

thin (~50 nm) Au or Pt film deposited on the Si prism (radius 22 mm, Pier optics) by electroless deposition [86, 87, 88]. The prism was then assembled to a three-electrode cell along with an Ag/AgCl reference electrode and a platinum wire counter electrode. The SEIRAS experiments were conducted on a FT-IR Vertex 70 (Bruker) FT-IR equipped with an MCT detector. The optical path was fully filled with N_2 gas. The FTIR spectra were acquired in the attenuated total reflection (ATR) mode using a single-reflection ATR accessory (Pike Vee-Max II, Pike Technologies) at an incident angle of 68 degrees. The spectral resolution was 4 cm^{-1} and the scan velocity was 7.5 kHz. Each spectrum was measured by superimposing 256 interferograms. During each experiment, O_2 was bubbled through the electrolyte, and the prism surface was then cleaned by cyclic voltammetry between 0 and 1.0 V_{RHE}. After cleaning, the spectra were collected while applying potentiostatic potentials. All spectra were presented in the form of absorbance according to $\log(I_0/I)$, where I_0 and I are the spectra of background (at open circuit potential) and at the potentiostatic potential, respectively. Details of *in situ* SEIRAS were described elsewhere [71, 86, 87].

FTIR frequency calculations

The computed the vibrational frequency shifts for hydrogen-bonded species were simulated by DFT from the vibrational frequencies of individual ionic liquid cations, and with interaction of individual cations with a H-bond from a nearby OH or OOH, in an explicit solvation model (PCM), and 2-Pentanone (dielectric constant=15.5) was used as solvent [89]. We used the B3LYP functional and 6-311++G** basis set, as implemented in the Gaussian (g16) suite [90].

Proton Vibration Wavefunction Calculation

The vibrational wavefunctions and energies were calculated from a series of proton potentials determined at different H-bonded species calculated for FTIR frequency, which represent the observed interfacial H-bond structure at equilibrium states. The 1D proton potentials were scanned using a reported method [7]. Then, the 1D vibrational wavefunctions and energies were calculated from the proton potential by solving the one-dimensional Schrödinger equation numerically using the Fourier Grid Hamiltonian Multiconfigurational Self-Consistent-Field (FGH-MCSCF) method [5, 91, 92]. The Boltzmann probability P_v was calculated from energies of different states and the $S_{v\mu}$ was obtained by integrating the overlap of reactant and product's wavefunction[69,93]. The calculation details was presented in Supplementary methods.

Author contributions: Y.S.H. and T.W conceived the idea and designed the experiments. T.W. carried out experiments on catalyst synthesis, electrocatalytic tests and data analysis. Y.Z. and T.W. performed the *in situ* surface-enhanced FT–IR spectroscopy measurements. Y.Z. and T.W performed the DFT calculations and analysis. T.W. and B.H. analyzed electrochemical data. B.C. synthesized nanoparticles and performed TEM test. R.R.R., L.G. and S.G.S. participated in the discussion and interpretation of experimental and theoretical data. Y.S.H. and T.W. wrote the manuscript. All of the authors discussed the results and commented on the manuscript.

Acknowledgement: This work was supported in part by the Toyota Research Institute through the Accelerated Materials Design and Discovery programme and the Skoltech-MIT Center for Electrochemical Energy. We thank Prof. Zhong-Qun Tian from Xiamen University for fruitful discussion. This work used the Extreme Science and Engineering Discovery Environment (XSEDE),

which is supported by National Science Foundation grant no. ACI-154856283. This research also used resources of the National Energy Research Scientific Computing Center (NERSC), a DOE Office of Science User Facility supported by the Office of Science of the US DOE under contract no. DE-AC02-05CH11231.

Reference

1. Benkovic SJ, Hammes-Schiffer S. A perspective on enzyme catalysis. *Science* 2003, **301**(5637)**:** 1196-1202.

2. Hammes-Schiffer S, Stuchebrukhov AA. Theory of coupled electron and proton transfer reactions. *Chem. Rev.* 2010, **110**(12)**:** 6939-6960.

3. Kretchmer JS, Boekelheide N, Warren JJ, Winkler JR, Gray HB, Miller TF, 3rd. Fluctuating hydrogen-bond networks govern anomalous electron transfer kinetics in a blue copper protein. *Proc. Natl. Acad. Sci. USA* 2018, **115**(24)**:** 6129-6134.

4. Weinberg DR, Gagliardi CJ, Hull JF, Murphy CF, Kent CA, Westlake BC*, et al.* Proton-coupled electron transfer. *Chem. Rev.* 2012, **112**(7)**:** 4016-4093.

5. Hammes-Schiffer S, Soudackov AV. Proton-coupled electron transfer in solution, proteins, and electrochemistry. *J. Phys. Chem. B* 2008, **112**(45)**:** 14108-14123.

6. Edwards SJ, Soudackov AV, Hammes-Schiffer S. Driving force dependence of rates for nonadiabatic proton and proton-coupled electron transfer: Conditions for inverted region behavior. *J. Phys. Chem. B* 2009, **113**(44)**:** 14545-14548.

7. Horvath S, Fernandez LE, Soudackov AV, Hammes-Schiffer S. Insights into proton-coupled electron transfer mechanisms of electrocatalytic H2 oxidation and production. *Proc. Natl. Acad. Sci. USA* 2012, **109**(39)**:** 15663-15668.

8. Mayer JM. Proton-coupled electron transfer: a reaction chemist's view. *Annu. Rev. Phys. Chem.* 2004, **55:** 363-390.

9. Koper MT. Theory of multiple proton–electron transfer reactions and its implications for electrocatalysis. *Chem. Sci.* 2013, **4**(7)**:** 2710-2723.

10. Morris AJ, Meyer GJ, Fujita E. Molecular approaches to the photocatalytic reduction of carbon dioxide for solar fuels. *Acc. Chem. Res.* 2009, **42**(12)**:** 1983-1994.

11. Hammarström L. Accumulative charge separation for solar fuels production: coupling light-induced single electron transfer to multielectron catalysis. *Acc. Chem. Res.* 2015, **48**(3)**:** 840-850.

12. Mora SJ, Odella E, Moore GF, Gust D, Moore TA, Moore AL. Proton-coupled electron transfer in artificial photosynthetic systems. *Acc. Chem. Res.* 2018, **51**(2)**:** 445-453.

13. Meyer TJ, Huynh MHV, Thorp HH. The possible role of proton-coupled electron transfer (PCET) in water oxidation by photosystem II. *Angew. Chem. Int. Ed.* 2007, **46**(28)**:** 5284-5304.

14. Nørskov JK, Rossmeisl J, Logadottir A, Lindqvist L, Kitchin JR, Bligaard T*, et al.* Origin of the overpotential for oxygen reduction at a fuel-cell cathode. *J. Phys. Chem. B* 2004, **108**(46)**:** 17886-17892.

15. Viswanathan V, Hansen HA, Rossmeisl J, Nørskov JK. Unifying the 2e–and 4e–reduction of oxygen on metal surfaces. *J. Phys. Chem. Lett.* 2012, **3**(20)**:** 2948-2951.

16. Ohta N, Nomura K, Yagi I. Adsorption and Electroreduction of Oxygen on Gold in Acidic Media: In Situ Spectroscopic Identification of Adsorbed Molecular Oxygen and Hydrogen Superoxide. *J. Phys. Chem. C* 2012, **116**(27)**:** 14390-14400.

17. Shao MH, Adzic RR. Spectroscopic identification of the reaction intermediates in oxygen reduction on gold in alkaline solutions. *J. Phys. Chem. B* 2005, **109**(35)**:** 16563-16566.

18. Casalongue HS, Kaya S, Viswanathan V, Miller DJ, Friebel D, Hansen HA*, et al.* Direct observation of the oxygenated species during oxygen reduction on a platinum fuel cell cathode. *Nat. Commun.* 2013, **4**(1)**:** 1-6.

19. Dong J-C, Zhang X-G, Briega-Martos V, Jin X, Yang J, Chen S*, et al.* In situ Raman spectroscopic evidence for oxygen reduction reaction intermediates at platinum single-crystal surfaces. *Nat. Energy* 2019, **4**(1)**:** 60-67.

20. Kulkarni A, Siahrostami S, Patel A, Nørskov JK. Understanding catalytic activity trends in the oxygen reduction reaction. *Chem. Rev.* 2018, **118**(5)**:** 2302-2312.

21. Hansen HA, Viswanathan V, Nørskov JK. Unifying kinetic and thermodynamic analysis of 2 e– and 4 e–reduction of oxygen on metal surfaces. *J. Phys. Chem. C* 2014, **118**(13)**:** 6706-6718.

22. Mavrikakis M, Hammer B, Nørskov JK. Effect of strain on the reactivity of metal surfaces. *Phys. Rev. Lett.* 1998, **81**(13)**:** 2819.

23. Strasser P, Koh S, Anniyev T, Greeley J, More K, Yu C*, et al.* Lattice-strain control of the activity in dealloyed core–shell fuel cell catalysts. *Nat. Chem.* 2010, **2**(6)**:** 454.

24. Kitchin J, Nørskov JK, Barteau M, Chen J. Modification of the surface electronic and chemical properties of Pt (111) by subsurface 3d transition metals. *J. Chem. Phys.* 2004, **120**(21)**:** 10240-10246.

25. Bligaard T, Nørskov JK. Ligand effects in heterogeneous catalysis and electrochemistry. *Electrochim. Acta* 2007, **52**(18)**:** 5512-5516.

26. Li D, Wang C, Strmcnik DS, Tripkovic DV, Sun X, Kang Y*, et al.* Functional links between Pt single crystal morphology and nanoparticles with different size and shape: the oxygen reduction reaction case. *Energy Environ. Sci.* 2014, **7**(12)**:** 4061-4069.

27. Calle-Vallejo F, Tymoczko J, Colic V, Vu QH, Pohl MD, Morgenstern K*, et al.* Finding optimal surface sites on heterogeneous catalysts by counting nearest neighbors. *Science* 2015, **350**(6257)**:** 185-189.

28. Tian N, Zhou Z-Y, Sun S-G, Ding Y, Wang ZL. Synthesis of tetrahexahedral platinum nanocrystals with high-index facets and high electro-oxidation activity. *Science* 2007, **316**(5825)**:** 732-735.

29. Stamenkovic VR, Fowler B, Mun BS, Wang G, Ross PN, Lucas CA*, et al.* Improved oxygen reduction activity on Pt3Ni(111) via increased surface site availability. *Science* 2007, **315**(5811)**:** 493-497.

30. Escudero-Escribano M, Malacrida P, Hansen MH, Vej-Hansen UG, Velazquez-Palenzuela A, Tripkovic V*, et al.* Tuning the activity of Pt alloy electrocatalysts by means of the lanthanide contraction. *Science* 2016, **352**(6281)**:** 73-76.

31. Strmcnik D, Escudero-Escribano M, Kodama K, Stamenkovic VR, Cuesta A, Markovic NM. Enhanced electrocatalysis of the oxygen reduction reaction based on patterning of platinum surfaces with cyanide. *Nat. Chem.* 2010, **2**(10)**:** 880-885.

32. Snyder J, Fujita T, Chen MW, Erlebacher J. Oxygen reduction in nanoporous metal-ionic liquid composite electrocatalysts. *Nat. Mater.* 2010, **9**(11)**:** 904-907.

33. Strmcnik D, Kodama K, van der Vliet D, Greeley J, Stamenkovic VR, Markovic NM. The role of non-covalent interactions in electrocatalytic fuel-cell reactions on platinum. *Nat. Chem.* 2009, **1**(6)**:** 466-472.

34. Blizanac BB, Ross PN, Markovic NM. Oxygen electroreduction on Ag(111): The pH effect. *Electrochim. Acta* 2007, **52**(6)**:** 2264-2271.

35. Chen C, Kang Y, Huo Z, Zhu Z, Huang W, Xin HL*, et al.* Highly crystalline multimetallic nanoframes with three-dimensional electrocatalytic surfaces. *Science* 2014, **343**(6177)**:** 1339-

1343.

36. Zheng J, Sheng W, Zhuang Z, Xu B, Yan Y. Universal dependence of hydrogen oxidation and evolution reaction activity of platinum-group metals on pH and hydrogen binding energy. *Sci. Adv.* 2016, **2**(3)**:** e1501602.

37. Sheng W, Zhuang Z, Gao M, Zheng J, Chen JG, Yan Y. Correlating hydrogen oxidation and evolution activity on platinum at different pH with measured hydrogen binding energy. *Nat. Commun.* 2015, **6:** 5848.

38. Strmcnik D, van der Vliet DF, Chang KC, Komanicky V, Kodama K, You H*, et al.* Effects of Li+, K+, and Ba2+ Cations on the ORR at Model and High Surface Area Pt and Au Surfaces in Alkaline Solutions. *J. Phys. Chem. Lett.* 2011, **2**(21)**:** 2733-2736.

39. Ledezma-Yanez I, Wallace WDZ, Sebastián-Pascual P, Climent V, Feliu JM, Koper MTM. Interfacial water reorganization as a pH-dependent descriptor of the hydrogen evolution rate on platinum electrodes. *Nat. Energy* 2017, **2**(4).

40. Sheng W, Gasteiger HA, Shao-Horn Y. Hydrogen Oxidation and Evolution Reaction Kinetics on Platinum: Acid vs Alkaline Electrolytes. *J. Electrochem. Soc.* 2010, **157**(11)**:** B1529.

41. Koper MT. Theory of the transition from sequential to concerted electrochemical proton-electron transfer. *Phys. Chem. Chem. Phys.* 2013, **15**(5)**:** 1399-1407.

42. Li MF, Liao LW, Yuan DF, Mei D, Chen Y-X. pH effect on oxygen reduction reaction at Pt (1 1 1) electrode. *Electrochim. Acta* 2013, **110:** 780-789.

43. Duan Z, Henkelman G. Theoretical resolution of the exceptional oxygen reduction activity of Au (100) in alkaline media. *ACS Catal.* 2019, **9**(6)**:** 5567-5573.

44. Mei D, He ZD, Zheng YL, Jiang DC, Chen YX. Mechanistic and kinetic implications on the ORR on a Au(100) electrode: pH, temperature and H-D kinetic isotope effects. *Phys. Chem. Chem. Phys.* 2014, **16**(27)**:** 13762-13773.

45. Blizanac BB, Lucas CA, Gallagher ME, Arenz M, Ross PN, Marković NM. Anion Adsorption, CO Oxidation, and Oxygen Reduction Reaction on a Au(100) Surface: The pH Effect. *J. Phys. Chem. B* 2004, **108**(2)**:** 625-634.

46. Koper MTM. Volcano Activity Relationships for Proton-Coupled Electron Transfer Reactions in Electrocatalysis. *Top. Catal.* 2015, **58**(18-20)**:** 1153-1158.

47. Zhang GR, Munoz M, Etzold BJ. Accelerating Oxygen-Reduction Catalysts through Preventing Poisoning with Non-Reactive Species by Using Hydrophobic Ionic Liquids. *Angew. Chem. Int. Ed.* 2016, **55**(6)**:** 2257-2261.

48. Chen C, Kang Y, Huo Z, Zhu Z, Huang W, Xin HL*, et al.* Highly crystalline multimetallic nanoframes with three-dimensional electrocatalytic surfaces. *Science* 2014, **343**(6177)**:** 1339-1343.

49. Zhang GR, Wolker T, Sandbeck DJS, Munoz M, Mayrhofer KJJ, Cherevko S*, et al.* Tuning the Electrocatalytic Performance of Ionic Liquid Modified Pt Catalysts for the Oxygen Reduction Reaction via Cationic Chain Engineering. *ACS Catal.* 2018, **8**(9)**:** 8244-8254.

50. Benn E, Uvegi H, Erlebacher J. Characterization of Nanoporous Metal-Ionic Liquid Composites for the Electrochemical Oxygen Reduction Reaction. *J. Electrochem. Soc.* 2015, **162**(10)**:** H759-H766.

51. Higgins EM, Sherwood JA, Lindsay AG, Armstrong J, Massey RS, Alder RW*, et al.* pKas of the conjugate acids of N-heterocyclic carbenes in water. *Chem. Commun.* 2011, **47**(5)**:** 1559-1561.

52. Kaupmees K, Trummal A, Leito I. Basicities of Strong Bases in Water: A Computational Study. *Croat. Chem. Acta* 2014, **87**(4)**:** 385-395.

53. Otake Y, Nakamura H, Fuse S. Rapid and Mild Synthesis of Amino Acid N -Carboxy Anhydrides: Basic-to-Acidic Flash Switching in a Microflow Reactor. *Angew. Chem. Int. Ed.* 2018, **130**(35)**:** 11559-11563.

54. Spialter L, Moshier RW. Amines. IV. The Base Strengths of Tetramethylated 1,2-Ethanediamines1. *J. Am. Chem. Soc.* 1957, **79**(22)**:** 5955-5957.

55. Tehan BG, Lloyd EJ, Wong MG, Pitt WR, Gancia E, Manallack DT. Estimation of pKa Using Semiempirical Molecular Orbital Methods. Part 2: Application to Amines, Anilines and Various Nitrogen Containing Heterocyclic Compounds. *Quantitative Structure-Activity Relationships* 2002, **21**(5)**:** 473-485.

56. Wang J, Markovic N, Adzic R. Kinetic analysis of oxygen reduction on Pt (111) in acid solutions: intrinsic kinetic parameters and anion adsorption effects. *J. Phys. Chem. B* 2004, **108**(13)**:** 4127-4133.

57. Garsany Y, Baturina OA, Swider-Lyons KE, Kocha SS. Experimental methods for quantifying the activity of platinum electrocatalysts for the oxygen reduction reaction. *Anal. Chem.* 2010, **82**(15)**:** 6321-6328.

58. Gasteiger HA, Kocha SS, Sompalli B, Wagner FT. Activity benchmarks and requirements for Pt, Pt-alloy, and non-Pt oxygen reduction catalysts for PEMFCs. *Appl. Catal. B* 2005, **56**(1-2)**:** 9-35.

59. Mayrhofer KJJ, Strmcnik D, Blizanac BB, Stamenkovic V, Arenz M, Markovic NM. Measurement of oxygen reduction activities via the rotating disc electrode method: From Pt model surfaces to carbon-supported high surface area catalysts. *Electrochim. Acta* 2008, **53**(7)**:** 3181-3188.

60. Sheng W, Chen S, Vescovo E, Shao-Horn Y. Size Influence on the Oxygen Reduction Reaction Activity and Instability of Supported Pt Nanoparticles. *J. Electrochem. Soc.* 2011, **159**(2)**:** B96-B103.

61. Shinozaki K, Zack JW, Richards RM, Pivovar BS, Kocha SS. Oxygen Reduction Reaction Measurements on Platinum Electrocatalysts Utilizing Rotating Disk Electrode Technique. *J. Electrochem. Soc.* 2015, **162**(10)**:** F1144-F1158.

62. Warren JJ, Tronic TA, Mayer JM. Thermochemistry of proton-coupled electron transfer reagents and its implications. *Chem. Rev.* 2010, **110**(12)**:** 6961-7001.

63. Ford DC, Nilekar AU, Xu Y, Mavrikakis M. Partial and complete reduction of O2 by hydrogen on transition metal surfaces. *Surf. Sci.* 2010, **604**(19-20)**:** 1565-1575.

64. Chevalet J, Rouelle F, Gierst L, Lambert JP. Electrogeneration and some properties of the superoxide ion in aqueous solutions. *J. Electroanal. Chem. Interfacial Electrochem.* 1972, **39**(1)**:** 201-216.

65. Costentin C, Evans DH, Robert M, Saveant JM, Singh PS. Electrochemical approach to concerted proton and electron transfers. Reduction of the water-superoxide ion complex. *J. Am. Chem. Soc.* 2005, **127**(36)**:** 12490-12491.

66. Li X, Gewirth AA. Oxygen electroreduction through a superoxide intermediate on bi-modified Au surfaces. *J. Am. Chem. Soc.* 2005, **127**(14)**:** 5252-5260.

67. Edwards SJ, Soudackov AV, Hammes-Schiffer S. Driving force dependence of rates for nonadiabatic proton and proton-coupled electron transfer: conditions for inverted region behavior. *J. Phys. Chem. B* 2009, **113**(44)**:** 14545-14548.

68. Brzezinski B, Zundel G. Formation of hydrogen-bonded chains between strong N-base and N H acids — a FTIR study. *J. Mol. Struct.* 1998, **446**(3)**:** 199-207.

69. Moschovi AM, Ntais S, Dracopoulos V, Nikolakis V. Vibrational spectroscopic study of the protic ionic liquid 1-H-3-methylimidazolium bis(trifluoromethanesulfonyl)imide. *Vib. Spectrosc.* 2012, **63:** 350-359.

70. Begue D, Qiao GG, Wentrup C. Nitrile imines: matrix isolation, IR spectra, structures, and rearrangement to carbodiimides. *J. Am. Chem. Soc.* 2012, **134**(11)**:** 5339-5350.

71. Ataka K-i, Yotsuyanagi T, Osawa M. Potential-dependent reorientation of water molecules at an electrode/electrolyte interface studied by surface-enhanced infrared absorption spectroscopy. *J. Phys. Chem.* 1996, **100**(25)**:** 10664-10672.

72. Nakamoto K, Margoshes M, Rundle RE. Stretching Frequencies as a Function of Distances in Hydrogen Bonds. *J. Am. Chem. Soc.* 1955, **77**(24)**:** 6480-6486.

73. Steiner T. The Hydrogen Bond in the Solid State. *Angew. Chem. Int. Ed.* 2002, **41**(1)**:** 48-76.

74. Gilli P, Pretto L, Bertolasi V, Gilli G. Predicting Hydrogen-Bond Strengths from Acid− Base Molecular Properties. The p K a Slide Rule: Toward the Solution of a Long-Lasting Problem. *Acc. Chem. Res.* 2009, **42**(1)**:** 33-44.

75. Tripković V, Skúlason E, Siahrostami S, Nørskov JK, Rossmeisl J. The oxygen reduction reaction mechanism on Pt (1 1 1) from density functional theory calculations. *Electrochim. Acta* 2010, **55**(27)**:** 7975-7981.

76. Goldsmith ZK, Soudackov AV, Hammes-Schiffer S. Theoretical analysis of the inverted region in photoinduced proton-coupled electron transfer. *Faraday Discuss.* 2019, **216:** 363-378.

77. Polanyi JC. Some concepts in reaction dynamics. *Science* 1987, **236**(4802)**:** 680-690.

78. Ebrahimi M, Guo SY, McNab IR, Polanyi JC. “Early” and “Late” Barriers in Dissociative Attachment: Steering Surface Reaction. *J. Phys. Chem. Lett.* 2010, **1**(17)**:** 2600-2605.

79. Chalkley MJ, Del Castillo TJ, Matson BD, Peters JC. Fe-Mediated Nitrogen Fixation with a Metallocene Mediator: Exploring p Ka Effects and Demonstrating Electrocatalysis. *J. Am. Chem. Soc.* 2018, **140**(19)**:** 6122-6129.

80. Kilgore UJ, Roberts JA, Pool DH, Appel AM, Stewart MP, DuBois MR*, et al.* [Ni (PPh2NC6H4X2) 2] 2+ complexes as electrocatalysts for H2 production: effect of substituents, acids, and water on catalytic rates. *J. Am. Chem. Soc.* 2011, **133**(15)**:** 5861-5872.

81. Graham DJ, Nocera DG. Electrocatalytic H2 evolution by proton-gated hangman iron porphyrins. *Organometallics* 2014, **33**(18)**:** 4994-5001.

82. Margarit CG, Schnedermann C, Asimow NG, Nocera DG. Carbon dioxide reduction by iron hangman porphyrins. *Organometallics* 2018, **38**(6)**:** 1219-1223.

83. Peng S, Lee Y, Wang C, Yin H, Dai S, Sun S. A facile synthesis of monodisperse Au nanoparticles and their catalysis of CO oxidation. *Nano Res.* 2008, **1**(3)**:** 229-234.

84. Huddleston JG, Visser AE, Reichert WM, Willauer HD, Broker GA, Rogers RD. Characterization and comparison of hydrophilic and hydrophobic room temperature ionic

liquids incorporating the imidazolium cation. *Green Chem.* 2001, **3**(4)**:** 156-164.

85. Nakamoto H, Watanabe M. Bronsted acid-base ionic liquids for fuel cell electrolytes. *Chem. Commun.* 2007(24)**:** 2539-2541.

86. Miyake H, Ye S, Osawa M. Electroless deposition of gold thin films on silicon for surface-enhanced infrared spectroelectrochemistry. *Electrochem. Commun.* 2002, **4**(12)**:** 973-977.

87. Miki A, Ye S, Osawa M. Surface-enhanced IR absorption on platinum nanoparticles: an application to real-time monitoring of electrocatalytic reactions. *Chem. Commun.* 2002(14)**:** 1500-1501.

88. Wang H, Zhou Y-W, Cai W-B. Recent applications of in situ ATR-IR spectroscopy in interfacial electrochemistry. *Curr. Opin. Electrochem.* 2017, **1**(1)**:** 73-79.

89. Frisch M, Trucks G, Schlegel H, Scuseria G, Robb M, Cheeseman J*, et al.* Gaussian 09, Revision D. 01; Gaussian: Wallingford, CT, 2009.

90. Laury ML, Carlson MJ, Wilson AK. Vibrational frequency scale factors for density functional theory and the polarization consistent basis sets. *J. Comput. Chem.* 2012, **33**(30)**:** 2380-2387.

91. Hammes-Schiffer S. webPCET Application Server. http://webpcet.chem.yale.edu: Yale University; 2009.

92. Webb SP, Hammes-Schiffer S. Fourier grid Hamiltonian multiconfigurational self-consistent-field: A method to calculate multidimensional hydrogen vibrational wavefunctions. *J. Chem. Phys.* 2000, **113**(13)**:** 5214-5227.

93. Neyerlin K, Gu W, Jorne J, Gasteiger HA. Determination of catalyst unique parameters for the oxygen reduction reaction in a PEMFC. *J. Electrochem. Soc.* 2006, **153**(10)**:** A1955-A1963.

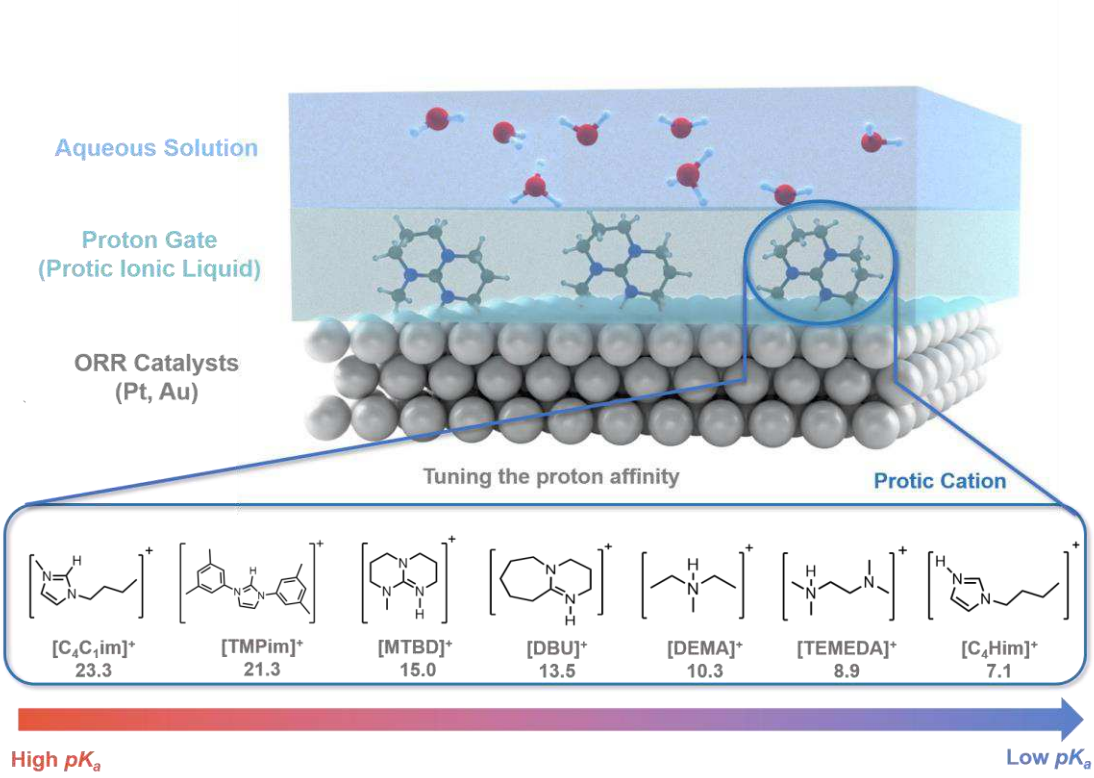

Scheme 1. Tuning local proton activity for ORR catalyzed on the surface of metallic catalysts by adding a thin layer of protic ionic liquids, where the pK_a value can range from 7.1 to 23.3 [51, 52, 53, 54, 55]. The anion of all ionic liquids used was NTf_2 in this work.

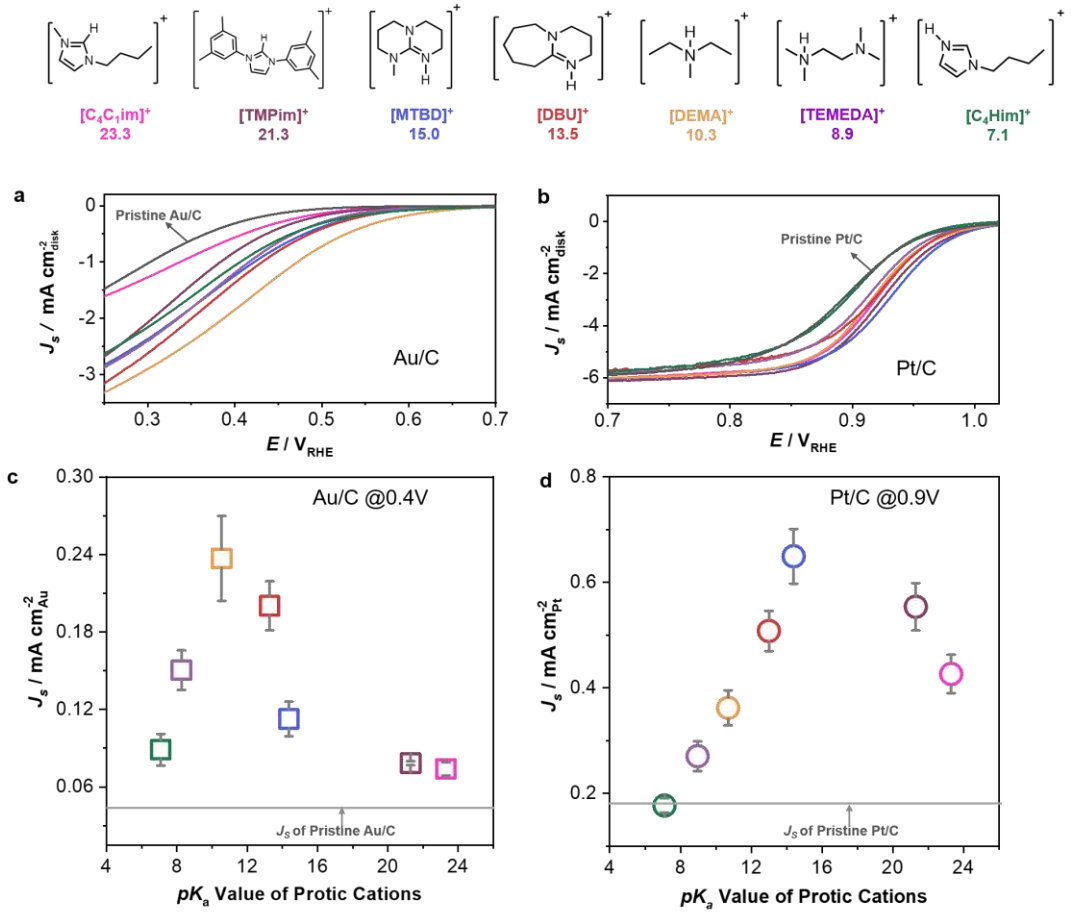

Fig.1 pK_a-dependent ORR activity on Au/C and Pt/C measured in O_2-saturated 0.1 M $HClO_4$, with a scan rate of 10 mV/s and the rotation speed is 1600 rpm. (a and b) Background and *IR* corrected ORR polarization curves of ionic-liquids-modified Au/C (a), Pt/C (b). (c and d) The relationship between the enhancement in ORR specific kinetic currents on ionic-liquids-modified Au/C (c), Pt/C (d) as a function of the pK_a value of protic cations in ionic liquids. Error bars represent standard deviations (SDs) of at least three independent measurements. The loading of Pt was controlled at 20 μg·cm^{-2} and the loading of Au were controlled at 40 μg·cm^{-2}. 0.05wt% Nafion was added to the catalytic layer.

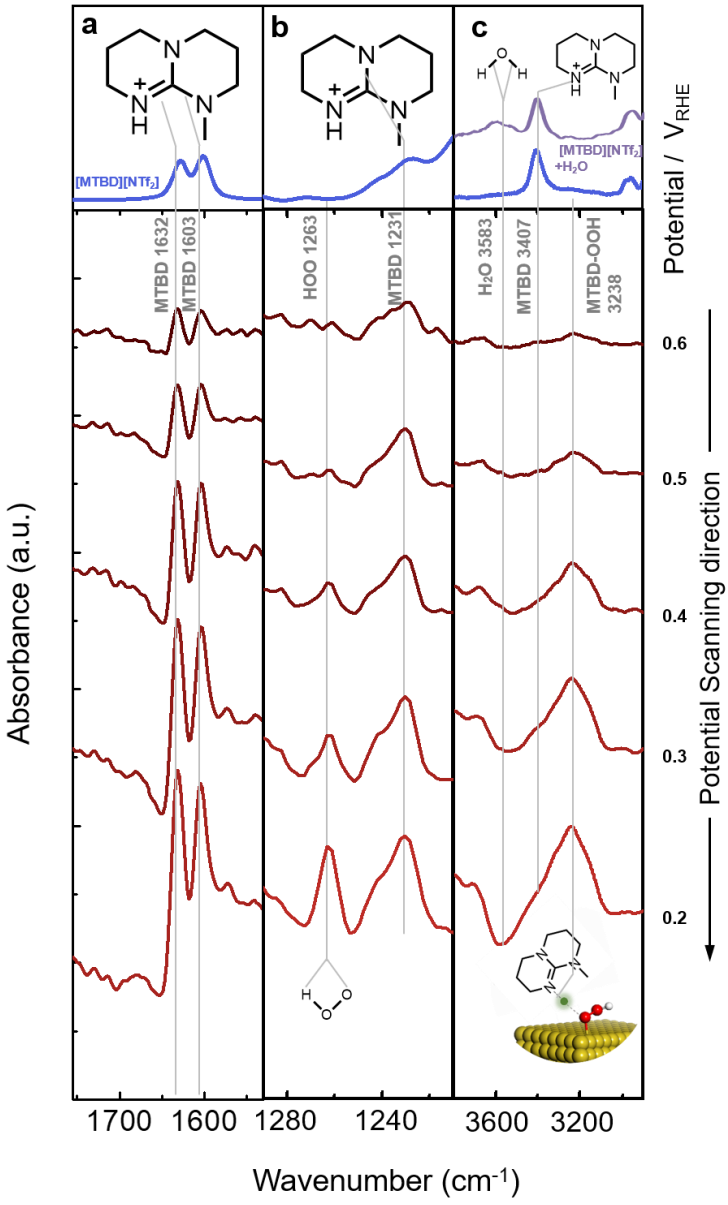

Fig. 2 *In situ* ATR-SEIRAS measurement on a [MTBD][NTf_2]-modified Au electrode in oxygen-saturated 0.1 M $HClO_4$. (a) C=N stretching region, (b) O-O-H bending region and (c) X-H (X=N, O) stretching region were obtained during potential steps swept from 0.2 V_{RHE} to 0.6 V_{RHE} in 0.1 M $HClO_4$. The blue curves show the IR spectrum of pristine [MTBD][NTf_2] and the purple curve shows the IR spectrum of pristine [MTBD][NTf_2] with 0.5M water. The cumulative number of 256 was used at a 4 cm^{-1} resolution. Spectra were subtracted with respect to a reference spectrum obtained at OCV in 0.1 M $HClO_4$.

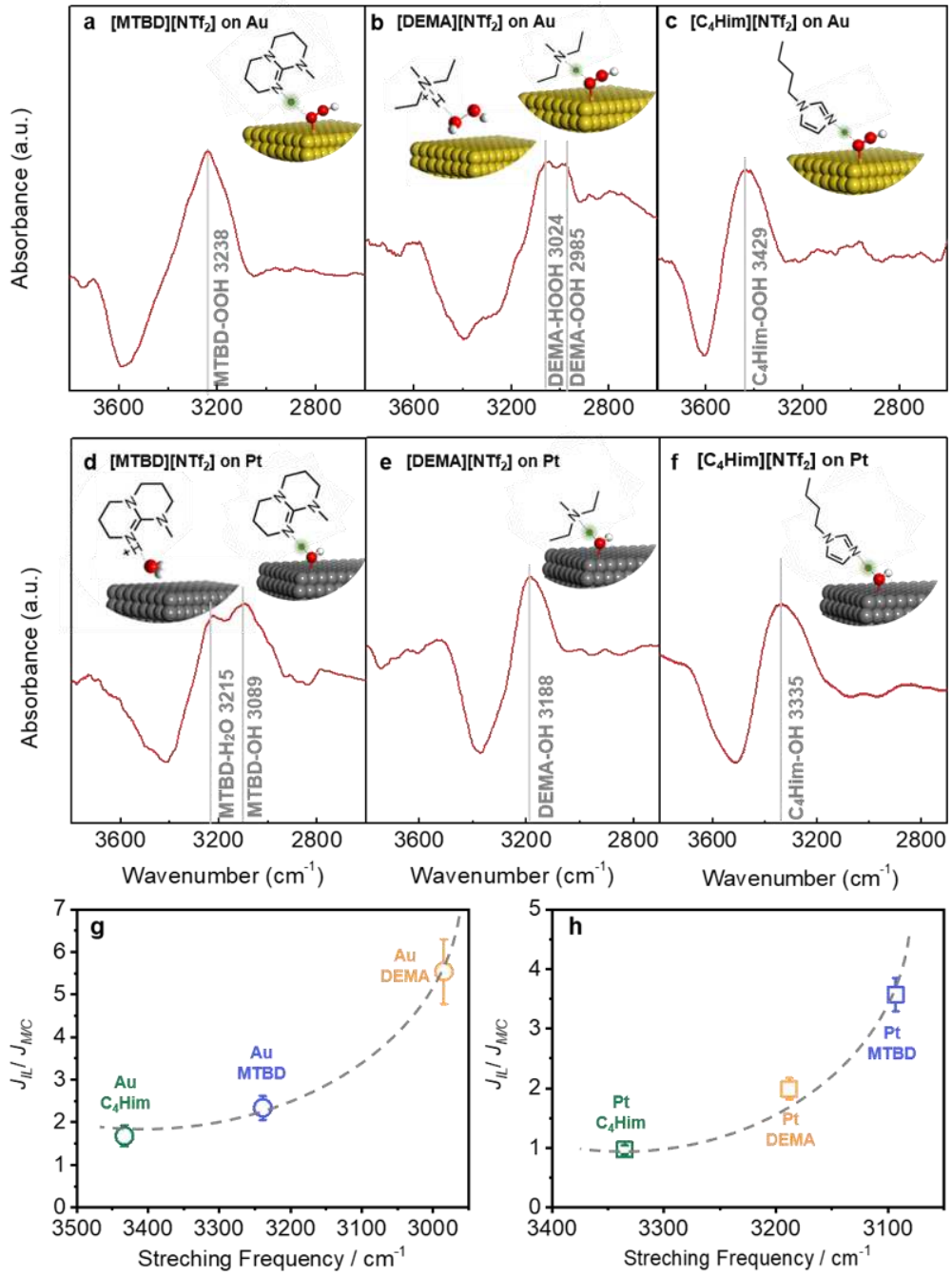

Fig. 3 *In situ* ATR-SEIRAS measurement on an ionic-liquid-modified Au and Pt electrode in 0.1 M $HClO_4$. X-H (X=N, O) stretching region of (a) [MTBD][NTf_2]-modified Au, (b) [DEMA][NTf_2]-modified Au, (c) [C_4Him][NTf_2]-modified Au, (d) [MTBD][NTf_2]-modified Pt, (e) [DEMA][NTf_2]-modified Pt and (f) [C_4Him][NTf_2]-modified Pt. The spectra were acquired at 0.2 V_{RHE} for Au and 0.5V_{RHE} for Pt. The peak

position of the H-bonded species indicates the strength of H-bond forming during the ORR process; (g, h) the relationship between the stretching frequency of the H-bonding species and the ionic liquid enhancement for ORR catalyzed by Au/C (g) and Pt/C (h), which is defined by $J_{IL\text{-}M/C}/J_{M/C}$ ($J_{IL\text{-}M/C}$ is the ORR current density of ionic-liquid-modified sample, $J_{M/C}$ is the current density of pristine Pt/C or Au/C). Error bars represent SDs of at least three independent measurements. The relationship indicates stronger H-bond would lead to higher ORR activity. The curve only serves as a guide to eyes.

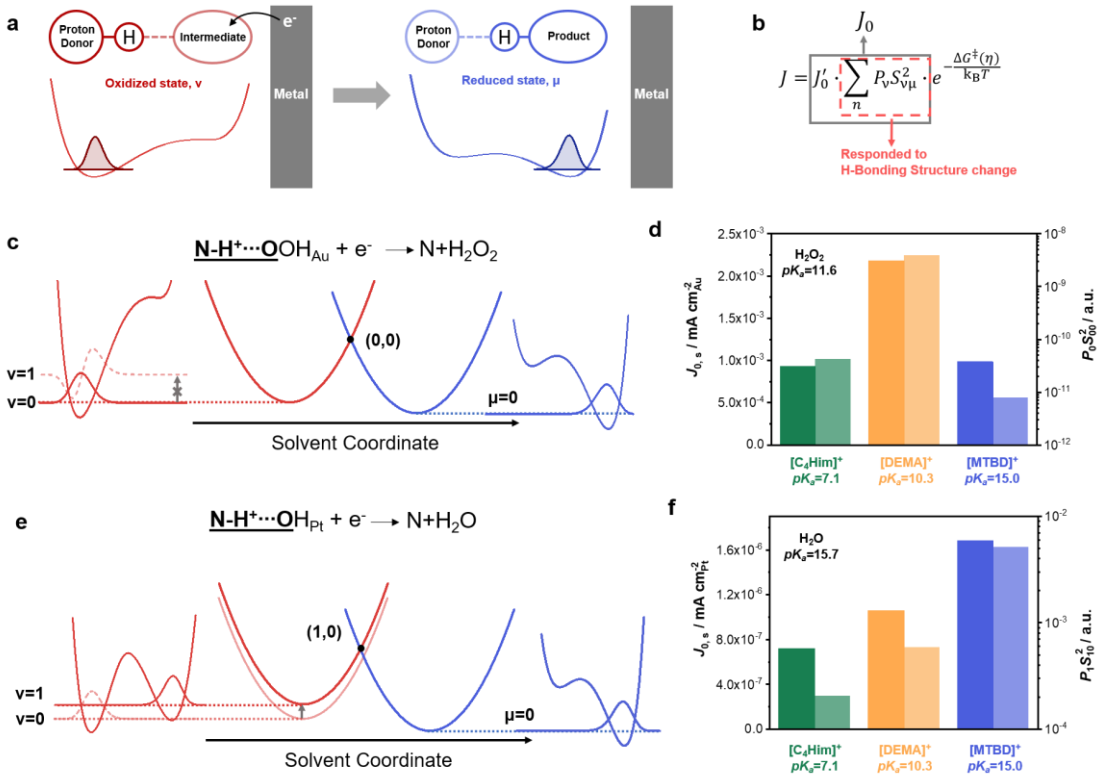

Fig. 4 Evaluating the structural effect of interfacial H-bond by calculating the vibrational wavefunction and energy levels for proton vibrational states of H-bonded species. (a) A scheme of the PCET reaction at H-bonded interface. The red and bule curves depict proton potential and proton wavefunction (shadowed curve) in ground state of reactant and product as functions of the proton coordinate. Proton is close to the proton donor in the reactant. After the H-bonded species get one electron from metal electrode, it will transfer to the proton acceptor in the product. The reaction kinetic is related with the integral overlap of wavefunctions between the reactant and product (denoted as $S_{\nu\mu}$) and Boltzmann probability of different vibronic states (denoted as P_ν). (b) the expression of current density exhibits that the J_0 (exchange current density) is proportional to $P_\nu S_{\nu\mu}^2$, which is dominated by H-bonding structure. (c, e) Schematic depiction of free energy surface for PCET reaction in $NH^+\cdots OOH_{Au}$ and $NH^+\cdots OH_{Pt}$. The Marcus parabolas of reactant (red) and product (blue) in the center frame illustrate the nonadiabatic transitions occur at the collective solvent coordinates across the

intersection (black points) of reactant and product parabolas. Proton potentials and proton wavefunctions in contributing state of reactant and product as functions of the proton coordinate are depicted in left (reactant) and right (product) frame. For $NH^+\cdots OOH_{Au}$ (c), the reactant ground state is the contributing state. For $NH^+\cdots OH_{Pt}$ (e), the 1st state of reactant is the contributing state. (d, f) The $P_{\nu}S_{\nu\mu}$ (in light color) of the contributing state for different ionic liquid cations interacting with OOH (d) and OH (f), comparing with the $J_{0,s}$ (specific exchange current density) (in dark color) extracted from Butler-Volmer equation for ORR on Pt (E, α is fixed to 1) [56, 91] and Au (E, α is fixed to 0.4).

Figures

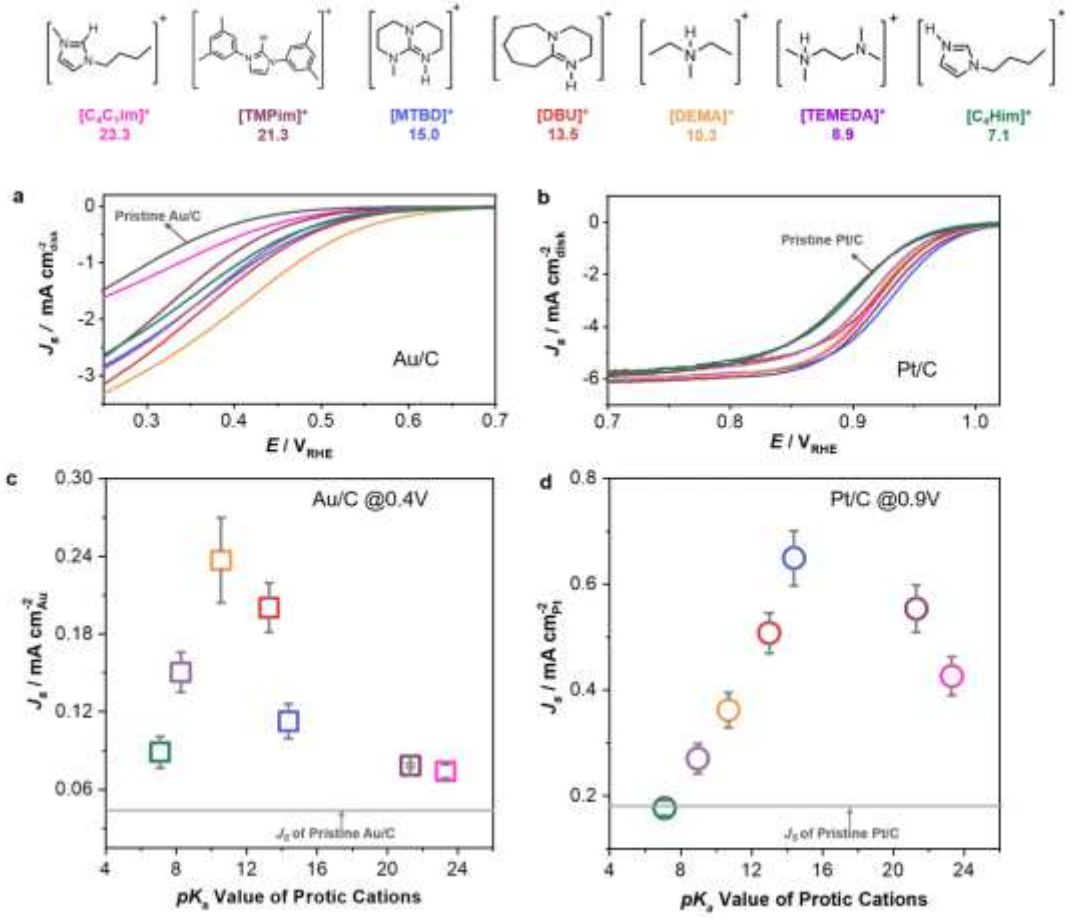

Figure 1

[Please see the manuscript file to view the figure caption.]

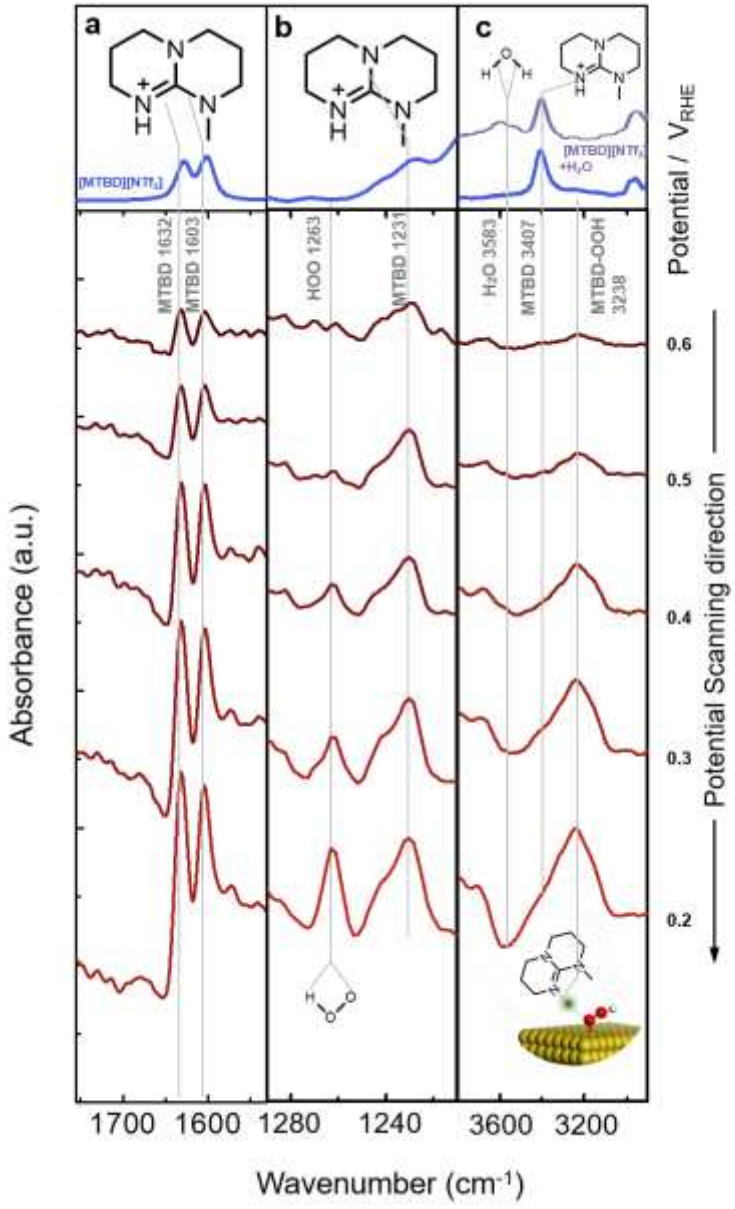

Figure 2

[Please see the manuscript file to view the figure caption.]

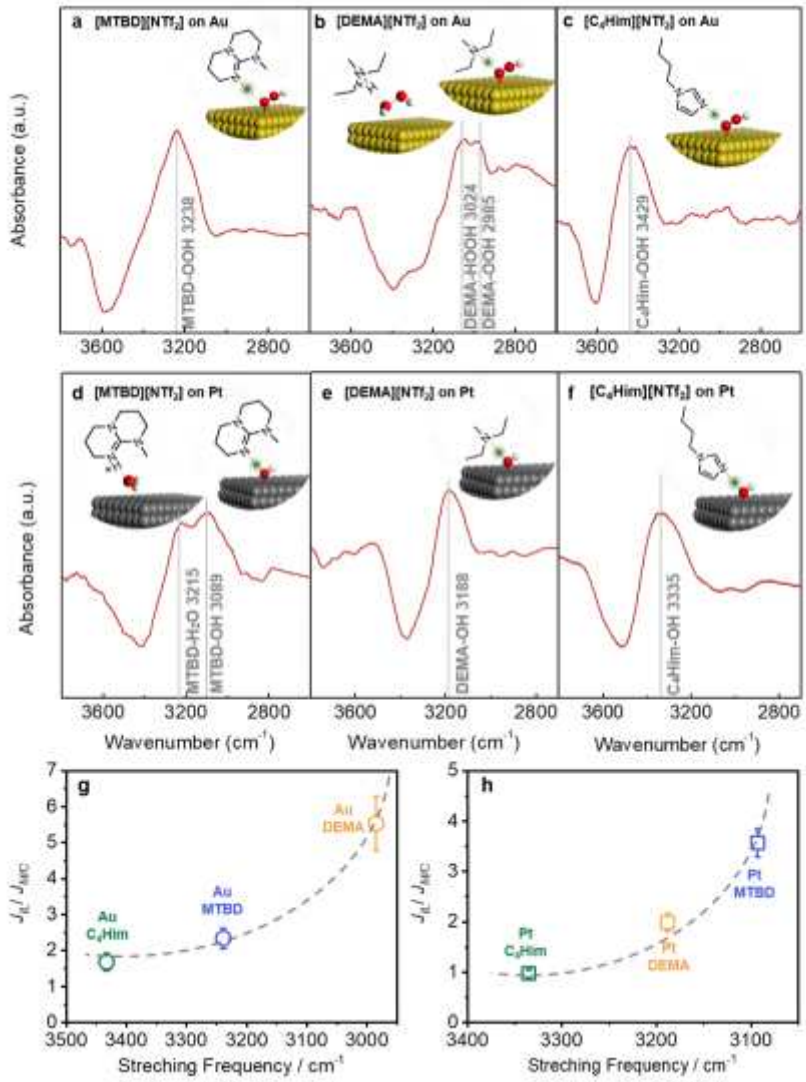

Figure 3

[Please see the manuscript file to view the figure caption.]

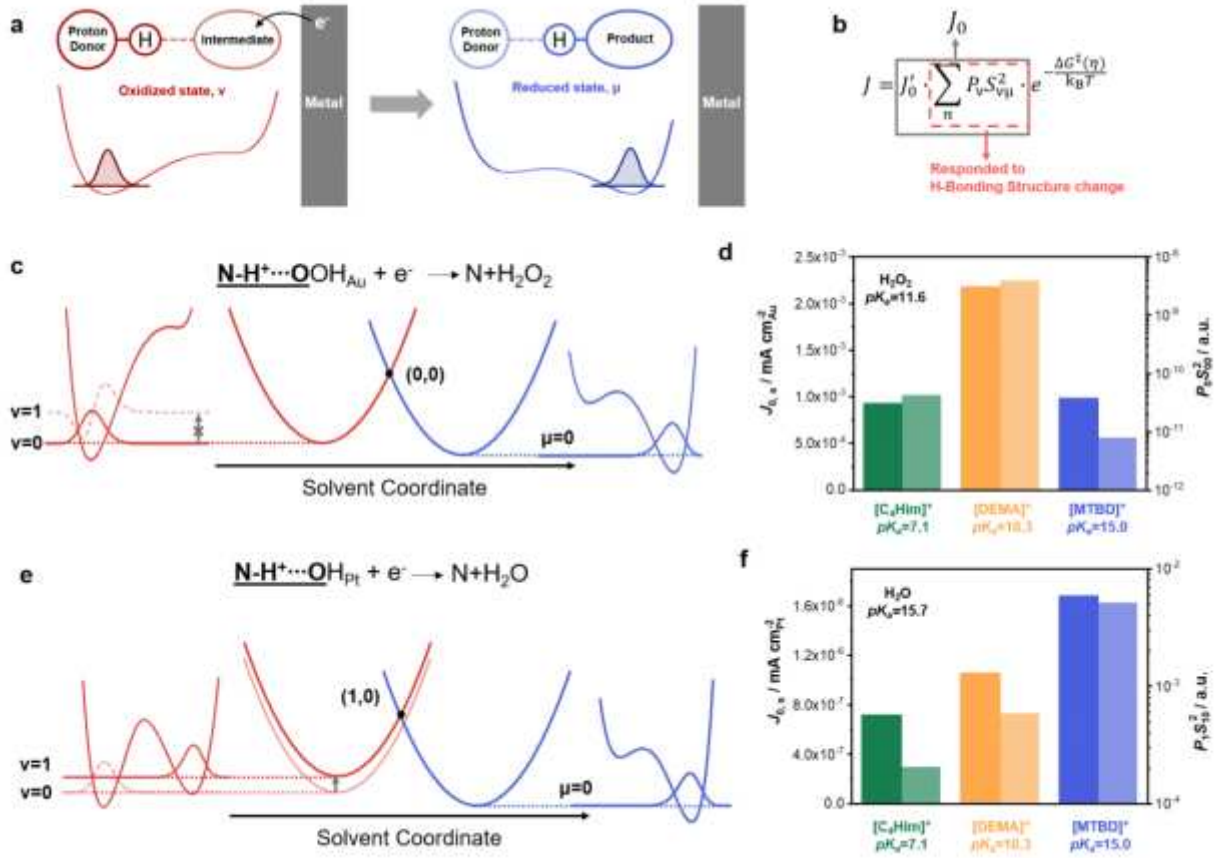

Figure 4

[Please see the manuscript file to view the figure caption.]

Supplementary Files

This is a list of supplementary files associated with this preprint. Click to download.

- SI.pdf